Spin-polarized current-induced excitations in a coupled magnetic layer system

D. Gusakova,[1,2,*,†] D. Houssameddine,[2] U. Ebels,[2] B. Dieny,[2] L. Buda-Prejbeanu,[2,3] M. C. Cyrille,[1] and B. Delaët[1]
[1]*CEA-LETI, MINATEC, DRT/LETI/DIHS, 17 Rue des Martyrs, 38054 Grenoble, France*
[2]*SPINTEC URA 2512 CEA-INAC/CNRS, 17 Rue des Martyrs, 38054 Grenoble, France*
[3]*Grenoble INP, 46, Avenue Félix Viallet, 38031 Grenoble Cedex 1, France*
(Received 17 October 2008; revised manuscript received 27 January 2009; published 9 March 2009)

The influence of dynamic interactions on the spin-polarized current-induced steady state oscillations has been studied numerically for a spin torque oscillator that is composed of a free layer and a synthetic antiferromagnetic (SAF) pinned layer. Two types of dynamical interactions have been considered. The first is the exchange interaction between the two layers that constitute the SAF pinned layer. The second is a mutual spin torque interaction between the free layer and the pinned SAF layer. Taking these interactions into account, the Landau-Lifshitz-Gilbert equation including the spin transfer torque has been solved simultaneously for all three layers in a macrospin approach. Besides the dynamic state diagram for such a coupled spin torque oscillator, three major results have been obtained for the dynamic excitation states: (1) the dynamic states are not in all cases steady state periodic oscillations but can present nonperiodic trajectories reminiscent of chaos, (2) due to the mutual spin torque interaction frequency jumps can occur which are interpreted in terms of resonance excitations and frequency locking between the free layer and SAF magnetizations, and (3) the acoustic-type steady state oscillations of the SAF differ from those of a single layer in that the frequency vs current dependence of the in-plane precession modes can show both redshift as well as blueshift. This is interpreted as a general property of the large-angle nonlinear dynamics of a SAF.

DOI: 10.1103/PhysRevB.79.104406 PACS number(s): 72.25.Ba, 75.75.+a, 75.40.Gb, 78.20.Bh

I. INTRODUCTION

A spin-polarized electrical current can transfer spin angular momentum to a ferromagnet[1,2] which can be used to control the magnetization state of a magnetoresistive device. In particular it is possible to induce either a reversal of the magnetization,[3,4] which is of interest for magnetic memory devices, or it can induce large-angle periodic oscillations of the magnetization,[5–7] which is of interest for tunable microwave oscillator devices. Up to now the majority of experiments on spin transfer driven excitations have been performed on planar spin valve nanopillar or nanocontact structures[4,6–11] of the type polarizer/spacer/free layer, where the polarizer (Pol), i.e., the pinned layer and the free layer (FL), consist of a single in-plane magnetized ferromagnet.

The use in the experiments of a synthetic antiferromagnet (SAF) [see Fig. 1(a)] instead of a single ferromagnetic pinned layer insures a more rigid pinned layer alignment and minimizes the dipolar stray field on the free layer. Such a SAF consists of two in-plane magnetized ferromagnetic layers [bottom layer (BL) and top layer (TL)] that are exchange coupled via a Ruderman-Kittel-Kasuya-Yosida (RKKY) interaction[12] across a thin nonmagnetic spacer whose thickness is adjusted to produce an antiferromagnetic coupling in zero applied field. The corresponding exchange field used in spin valve and tunnel junction devices is usually of the order of a few kilo-Oersteds. Up to now, only few experimental studies on spin transfer driven excitations have been reported for which the polarizer is a synthetic antiferromagnet.[13–18] However the use of a SAF pinned layer gains more attention since, for example, it is part of most tunnel junction devices which are quite promising due to the enhanced output power.[15–18] Furthermore, recent experiments[15,18,19] have shown that it is possible to induce excitations not only in the free layer but also in the pinned SAF layer under specific conditions. Similarly, in our group narrow and intense microwave emission peaks were observed in a spin valve structure that are attributed to SAF excitations in zero or larger applied field.[20] This makes the use of SAF excitations potentially interesting for applications. It will therefore be of importance to understand the spin-polarized current-induced dynamics of such a structure, which is the aim of this paper.

In contrast to most theoretical descriptions that have considered the spin-polarized current-induced free layer dynamics only,[21–23] here we discuss the free layer and pinned layer dynamics simultaneously in a macrospin description and address two specific aspects of the magnetization dynamics including interactions: (i) the spin-polarized current-induced excitations of an antiparallel RKKY exchange-coupled two layer system, such as the SAF, for three different field regions (antiparallel plateau, spin flop, and saturation, see Sec. II) and (ii) the effect of dynamic interactions between the free and pinned layers that are due to the reciprocal spin transfer torque. The latter choice needs some justification since in principle one also should consider dynamic dipolar interactions between the different layers. One of the main motivations for including only the mutual spin torque interaction was that such an interaction has not been considered up to now for the asymmetric free layer–pinned layer system that we consider here. To our knowledge there is only one previous theoretical study that treats such a dynamic interaction in the limit of a symmetric structure[24] at small precession angles. In the case considered here, the first issue was therefore to check whether mutual spin torque interaction will affect the magnetization dynamics of the free or the pinned layer. The presented results are thus a first numerical verification of this important issue. Furthermore, we believe that the obtained results can be generalized to other dynamic interactions (such as dipolar) for which similar effects such

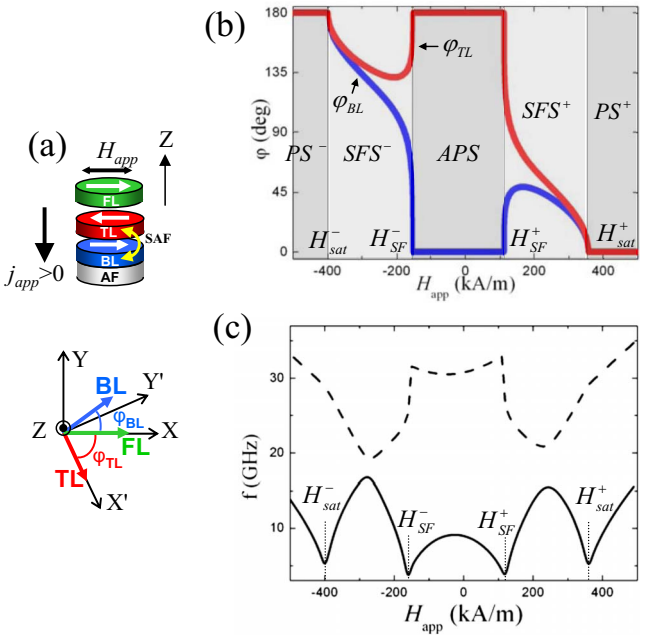

FIG. 1. (Color online) (a) Schematics of the planar oscillator configuration and the *X*-*Y*-*Z* coordinate system. Throughout the paper the blue/red/green colors are used to indicate the BL/TL/FL properties, respectively. (b) In-plane angles φ_{TL} (red) and φ_{BL} (blue) between the *X* axis and the TL and BL magnetizations as a function of applied field. PS, APS, and SFS abbreviations relate, correspondingly, to the parallel, antiparallel, and spin-flop regions stable states. (c) Ferromagnetic resonance frequencies of the SAF structure vs applied field (solid line: acoustic mode, dashed line: optic mode). The corresponding TL and BL parameters used in plots (b) and (c) are summarized in Table I and $J_{RKKY}=-1$ mJ/m^2.

as discussed in Secs. IV and V are expected; the difference being the precise current and field ranges and coupling strengths where such effects occur. Finally, since the SAF is almost compensated, the dipolar interaction on the free layer should be much reduced.

This paper is organized as follows. Section II presents simplified analytical expressions in a macrospin description for the stability of the static states as a function of current and applied field. In Sec. III we describe the current-field state diagram calculated numerically of a three layer system, coupled via exchange interaction (TL and BL of the SAF) and via spin transfer torque (FL and TL). In Sec. IV we present general aspects of the precession trajectories and in Sec. V the frequencies of the periodic steady state precession as a function of applied current and applied field.

II. ANALYTICAL CRITICAL BOUNDARIES

The oscillator configuration investigated here is presented in Fig. 1(a). It consists of a FL that is separated by a spacer from the SAF pinned layer structure. The SAF itself consists of two ferromagnetic layers that are called TL, for the one that is closest to the free layer, and BL. The BL is coupled to the TL by RKKY-exchange interaction and is also exchange biased by an antiferromagnet (AF).

In a first approach we will provide approximate analytical equations for the boundary of stability under spin torque of the FL and the SAF static states. These will be compared in Sec. III to numerical solutions of the Landau-Lifshitz-Gilbert (LLG) equation in a macrospin approach. While in the numerical solution the stability and dynamics of all three interacting layers (free layer and both SAF layers) can be investigated simultaneously, for the analytical studies we have to distinguish two simplifying cases:

(a) only the magnetization of the top SAF layer TL is experiencing a spin torque, while the BL and the FL magnetizations remain fixed with the FL playing the role of the polarizer;

(b) only the magnetization of the FL is experiencing a spin torque, while the SAF magnetization remains fixed, with the TL playing the role of the polarizer.

A. Static states of the SAF

In both cases, the zero current static configurations of all three layers need to be known. These are obtained from minimization of the energy density that contains contributions from the external field H_{app}, the RKKY interaction, the exchange bias field H_{ex}, the uniaxial in-plane shape anisotropy, and the out-of-plane demagnetization field H_d (see Appendix A). The uniaxial easy axes as well as the applied bias field are both directed along the in-plane *X* axis [see Fig. 1(a)]. The RKKY-type interlayer exchange coupling between the BL and TL of the SAF is parameterized by the bilinear coupling constant J_{RKKY}.[12,25,26] While the FL magnetization is always collinear with the anisotropy field and the applied field, three zero current magnetization configurations need to be distinguished for the magnetization of the SAF layers as a function of applied field amplitude:[25]

(i) *Plateau region* for $H^-_{SF}<H_{app}<H^+_{SF}$. The TL and BL magnetizations are collinear with the anisotropy field. However, the RKKY-type exchange coupling is chosen such that both layers are antiparallel to each other in zero and in low applied fields up to the spin-flop field H_{SF}. Due to the antiferromagnetic exchange bias of the BL (set into the positive *X* direction) the positive H^+_{SF} and negative H^-_{SF} spin-flop fields have different values, with $|H^+_{SF}|<|H^-_{SF}|$. As shown in Fig. 1(b) the corresponding in-plane equilibrium angles in the plateau region are $\varphi_{TL}=180°$ and $\varphi_{BL}=0°$ for the TL and BL, respectively, corresponding to the in-plane equilibrium configuration noted as antiparallel stable state (APS).

(ii) *Spin-flop region* $|H^\pm_{SF}|<|H_{app}|<|H^\pm_{sat}|$. At the spin-flop fields $H^\pm_{SF}$ the magnetizations of the TL and BL switch more or less gradually away from the in-plane easy axis and away from the antiparallel alignment, with both layers rotating toward the applied field direction upon increasing bias field. In Fig. 1(b) we label the corresponding in-plane configuration as SFS (for spin-flop stable state). The corresponding static equilibrium angles with $\varphi_{TL}<180°$ and $\varphi_{BL}>0°$ are calculated numerically and are given in Fig. 1(b) for a slightly uncompensated SAF (i.e., the product of $M_S d$ is almost the same with *d* the film thickness). As a consequence, when increasing the field toward positive saturation, the TL magnetization switches from $\varphi_{TL}=180°$ to $\varphi_{TL}=0°$ passing

through 90°. In contrast, when increasing the field amplitude toward negative saturation, it is the BL that rotates from $\varphi_{BL}=0°$ to $\varphi_{BL}=180°$ while the TL magnetization first rotates away but then comes back to 180° without passing through 90°. This asymmetry of the TL rotation in positive and negative fields has an important consequence for the symmetry of the stability diagram as discussed in Sec. II D.

(iii) *Saturation region* $|H_{app}|>|H_{sat}^{\pm}|$. For field values that are larger than the saturation field $H_{sat}^{\pm}$, the magnetizations of the TL and BL align parallel to the applied field. We label the corresponding in-plane configuration as PS in Fig. 1(b) (for parallel stable state), with $\varphi_{TL}=\varphi_{BL}=180°$ for negative field and $\varphi_{TL}=\varphi_{BL}=0°$ for positive field.

The analytical expressions of the spin-flop fields and the saturation fields are given in Appendix A, as calculated from the minimization of the energy density. It is noted that in this paper we describe a SAF structure for which we have $|H_{SF}^{\pm}|<|H_{sat}^{\pm}|$ as a result of the relatively strong RKKY-exchange energy of $J_{RKKY}=-1$ mJ/m^2 which has been chosen to be close to the experimental values.[20]

B. Critical currents for the SAF for $H_{app}>0$

The critical currents for which the static states of the TL (case a) or the FL (case b) become unstable are summarized in Fig. 2. They are derived upon linearization of the LLG equation enhanced by the Slonczewski spin torque term (called LLGS in the following) around the static equilibrium positions of the TL or the FL magnetization, respectively.[1,23,27,28] Here, the LLGS equation is given by

$$\frac{\partial \mathbf{m}}{\partial t} = -\gamma \mathbf{m} \times \mathbf{H}_{eff} + \alpha \mathbf{m} \times \frac{\partial \mathbf{m}}{\partial t} + \mathrm{STT},$$

$$\text{with} \quad \mathrm{STT} = \gamma j_{app} G(\eta,\theta)\mathbf{m} \times (\mathbf{m} \times \mathbf{p}), \tag{1}$$

where $\mathbf{m}$ is the normalized magnetization vector $\mathbf{m}=\mathbf{M}/M_S$ of the TL or FL, respectively, M_S is the corresponding saturation magnetization, γ is the corresponding gyromagnetic ratio, α is the corresponding Gilbert damping constant, j_{app} is the applied current, and $\mathbf{p}$ is the spin-polarization unit vector. The prefactor

$$G(\eta,\theta) = \frac{\hbar[-4+0.25\eta^{-3/2}(1+\eta)^3(3+\cos\theta)]^{-1}}{2e\mu_0 M_S d} \tag{2}$$

depends on the electron charge e, the layer thickness d, the angle θ between the magnetization unit vector $\mathbf{m}$ and the spin-polarization unit vector $\mathbf{p}$, and the spin torque efficiency η.

We start with the stability analysis of the SAF-TL (case a), for which we assume that the spacer between the TL and BL reduces considerably the spin polarization. Consequently the BL is not subjected to a spin torque and its magnetization be can supposed to be fixed along its equilibrium in-plane position, shown in Fig. 1(b). In this approximation the instability of the in-plane state of the TL determines the critical currents of the whole SAF structure. For this case the effective field H_{eff} in Eq. (1) includes an in-plane anisotropy field H_{an}, an out-of-plane demagnetizing field H_d, and the RKKY-type coupling field H_{RKKY} (see Appendix A).

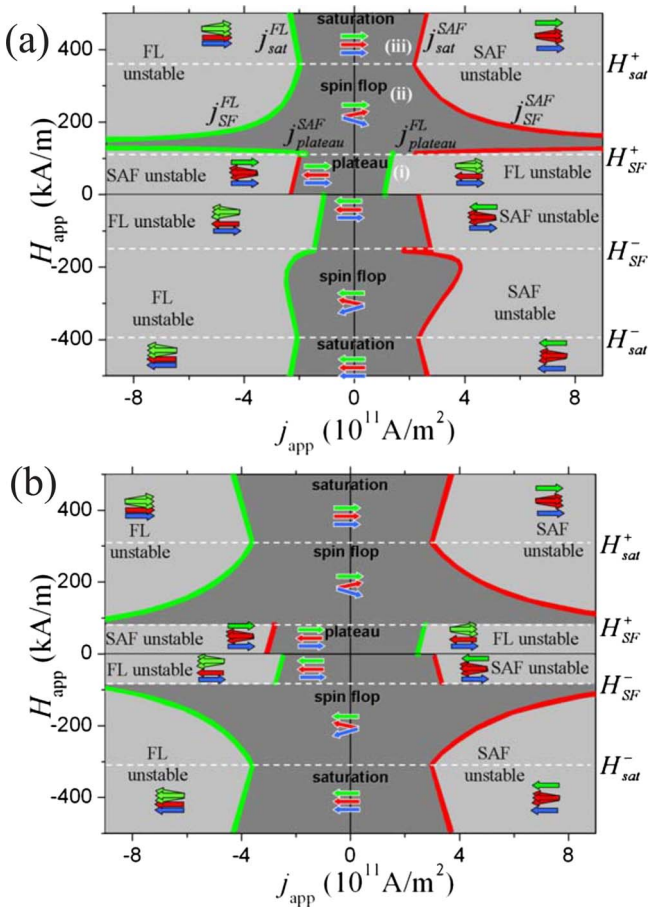

FIG. 2. (Color online) Critical currents vs applied field calculated analytically using Eqs. (3)–(8). (a) The case of an uncompensated SAF structure. The parameters for the BL/TL/FL layers are M_S (kA/m) 1600/1340/1070, K (J/m^3) 8000/6700/5350, d (nm) 2.5/3/3, $H_{ex}=40$ kA/m, and (N_x,N_y,N_z) (0.045,0.053,0.901)/(0.051,0.06,0.887)/(0.051,0.06,0.887). The critical fields are $H_{sat}^{+}=358$ kA/m, $H_{SF}^{+}=112$ kA/m, $H_{SF}^{-}=-154$ kA/m, and $H_{sat}^{-}=-398$ kA/m. (b) The case of a compensated SAF structure with M_S (kA/m) 1600/1600/1070, K (J/m^3) 8000/8000/5350, d (nm) 3/3/3, and (N_x,N_y,N_z) (0.045,0.053,0.901)/(0.045,0.053,0.901)/(0.051,0.06,0.887). The exchange bias is zero in case (b). In cases (a) and (b) the RKKY coupling constant is $J_{RKKY}=-1$ mJ/m^2, the spin torque coefficient is $G=1$ and $\alpha=0.02$. The arrows indicate the FL (green), TL (red), and BL (blue) magnetization alignment in the respective field regions [cf. Fig. 1(a)]. The red (green) lines indicate the critical current for which the SAF (FL) static states become unstable.

For simplicity in the following analytical calculations we discuss the range of positive applied field and the case of parallel alignment of the FL magnetization with the X axis. The calculation for negative applied field and opposite FL orientation may be carried out in a similar manner. In our configuration positive current corresponds to electrons flowing from the SAF to the FL [Fig. 1(a)]. Furthermore, in this analytical description we do not take the angular dependence of $G(\eta,\theta)$ into account, which is therefore constant, i.e., $G(\eta,\theta)=G=\text{const}$.

The linearization of LLGS for the TL magnetization dynamics is carried out in the local coordinate system $(X',Y',Z'=Z)$ which is obtained upon rotation by φ_{TL} of the (X,Y,Z) coordinate system around the Z axis, so that the X' axis coincides with the static equilibrium position of the TL [see Fig. 1(a)]. Projecting the LLGS equation onto the three axis X', Y', and Z', we obtain linearized equations for the local transverse magnetization components m_y' and m_z'. Details are given in Appendix B. The general solutions for m_y' and m_z' are of the form $A\exp(k_1t)+B\exp(k_2t)$. The condition of instability of the given magnetic configuration is obtained from the change of sign of the real part of the eigenvalues k_1 and k_2. Here a positive sign means that the amplitude of motion of **m** increases in time which corresponds to instability of the initial configuration.

For positive applied fields $H_{\mathrm{app}}>0$ we obtain the following expressions for the critical currents for the three field regions:

Saturation region (iii). In the saturation region, the TL and FL are parallel. The critical current above which the static state becomes unstable is given by

$$j_{\mathrm{sat}}^{\mathrm{SAF}}=\frac{\alpha}{G}\left(H_{\mathrm{app}}+H_{\mathrm{an}}+\frac{H_d}{2}-H_{\mathrm{RKKY}}\right). \tag{3}$$

The corresponding critical current $j_{\mathrm{sat}}^{\mathrm{SAF}}$ for a compensated SAF is indicated in Fig. 2(a) by the red line (SAF unstable) in region (iii). It is similar to the usual planar configuration in the parallel state, reflecting the similar initial parallel configuration. The difference being that here the RKKY-exchange field reduces the critical current since it counteracts the applied field.

Plateau region (i). In the plateau region the TL and FL are antiparallel. The critical current below which the static state becomes unstable is given by

$$j_{\mathrm{plateau}}^{\mathrm{SAF}}=-\frac{\alpha}{G}\left(-H_{\mathrm{app}}+H_{\mathrm{an}}+\frac{H_d}{2}+H_{\mathrm{RKKY}}\right). \tag{4}$$

The corresponding critical line $j_{\mathrm{plateau}}^{\mathrm{SAF}}$ is shown in Fig. 2(a) by the red line (SAF unstable) in region (i) and is similar to the usual planar configuration in the antiparallel state, including an additional RKKY-exchange field term. As compared to the saturation region, instability occurs at the opposite sign of the current. Note that this relation is valid also in negative field on the whole plateau for $H_{\mathrm{SF}}^{-}<H_{\mathrm{app}}<H_{\mathrm{SF}}^{+}$, as long as the FL orientation does not switch.

Spin-flop region (ii). In the spin-flop region the TL and BL make a finite angle with respect to each other that decreases from 180° to zero upon increasing field [see Fig. 1(a)]. Due to the TL rotation the spin-polarization vector is here given by $\mathbf{p}=(\cos\varphi_{\mathrm{TL}},\sin\varphi_{\mathrm{TL}},0)$. As a consequence, the corresponding critical line is different from the collinear configuration and as a new result we obtain the critical current above which the static state becomes unstable as

$$j_{\mathrm{SF}}^{\mathrm{SAF}}=\frac{\alpha}{G\cos\varphi_{\mathrm{TL}}}\left((H_{\mathrm{app}}+H_{\mathrm{an}})\cos\varphi_{\mathrm{TL}}+\frac{H_d}{2}-H_{\mathrm{RKKY}}\cos(\varphi_{\mathrm{TL}}+\varphi_{\mathrm{BL}})\right). \tag{5}$$

The corresponding critical line $j_{\mathrm{SF}}^{\mathrm{SAF}}$ is shown in Fig. 2(a) by the red line (SAF unstable) in region (ii). It joins the critical line $j_{\mathrm{sat}}^{\mathrm{SAF}}$ at the saturation field H_{sat} and has thus the same sign as $j_{\mathrm{sat}}^{\mathrm{SAF}}$ but opposite sign than $j_{\mathrm{plateau}}^{\mathrm{SAF}}$. This change in sign at the positive spin-flop field is due to the switching of the TL magnetization from antiparallel to parallel to the FL magnetization [cf. Fig. 1(b)]. Note that in Eq. (5), the RKKY-exchange field term is scaled by the cosine of the angle between the TL and BL magnetizations, which is maximal when the TL and BL are parallel. Furthermore, the $\cos\varphi_{\mathrm{TL}}$ term in the denominator leads to a divergence of the critical current when the TL magnetization rotates perpendicular to the X axis (i.e., to the FL magnetization) at the spin-flop field. As a whole this results in a hyperbolical dependence of the critical current on H_{app}. In order to better illustrate this we will give the expression for a fully compensated SAF with identical parameters for the TL and BL so that here $\varphi_{\mathrm{TL}}=\varphi_{\mathrm{BL}}$. Their cosine is then proportional to the applied field, with

$$\cos\varphi_{\mathrm{TL}}=\cos\varphi_{\mathrm{BL}}=\frac{H_{\mathrm{app}}}{2H_{\mathrm{RKKY}}-H_{\mathrm{an}}}.$$

With this the analytical expression for the critical line transforms into

$$j_{\mathrm{SF}}^{\mathrm{SAF}}=\frac{\alpha}{G}\left(-a\,H_{\mathrm{app}}+b+\frac{c}{H_{\mathrm{app}}}\right). \tag{6}$$

The coefficients a, b, and c are given in Appendix C. The last and main term in this expression is inversely proportional to the applied field that leads to the hyperbolic dependence of the critical current as a function of field. Note that in case of a fully compensated SAF the divergence of the critical current occurs at zero applied field. However since $|H_{\mathrm{SF}}|$ is always larger than zero due to the anisotropy field we do not observe this divergence for a fully compensated SAF structure. In this case the critical current takes important but finite values close to spin-flop field [see Fig. 2(b)].

C. Critical currents for the FL for $H_{\mathrm{app}}>0$

We will now consider case (b) for which the TL of the SAF stays fixed and plays the role of the polarizer for the FL. As in Sec. II B for simplicity we discuss the range of positive applied field and the case of parallel alignment of the FL magnetization with the positive X axis in absence of applied current. Similarly, we will have to distinguish three field regions due to the reorientation of the TL magnetization (i.e., the polarizer orientation) as a function of field [see Fig. 1(b)]. By reiterating the stability analysis for the FL we obtain the corresponding critical currents for the plateau (i), saturation (iii), and spin flop (ii) regions in positive fields as

$$j_{\mathrm{plateau}}^{\mathrm{FL}}=\frac{\alpha}{G}\left(H_{\mathrm{app}}+H_{\mathrm{an}}+\frac{H_d}{2}\right), \tag{7}$$

$$j_{\mathrm{sat}}^{\mathrm{FL}}=\frac{-\alpha}{G}\left(H_{\mathrm{app}}+H_{\mathrm{an}}+\frac{H_d}{2}\right), \tag{8}$$

$$j_{\mathrm{SF}}^{\mathrm{FL}} = \frac{-\alpha}{G\cos\varphi_{\mathrm{TL}}}\left(H_{\mathrm{app}} + H_{\mathrm{an}} + \frac{H_d}{2}\right). \quad (9)$$

These relations can be derived from the corresponding ones of the SAF-TL by

(1) dropping the RKKY-exchange field term,

(2) interchanging the sign of the current for each field region,

(3) in the case of the plateau region changing also the sign of the applied field,

(4) in the case of the spin-flop region dropping the multiplicative cos term before $(H_{\mathrm{app}}+H_{\mathrm{an}})$, since the free layer remains parallel to its easy axis, and

(5) using the corresponding material parameters for G, α, H_{an}, and H_d.

The change of sign of H_{app} in the plateau region is due to the fact that in the case of the TL, the applied field counteracts the RKKY interaction, "softening" the internal field and thus destabilizing the TL orientation, while in the FL case the applied field stabilizes the FL orientation.

As in the TL case, at the spin-flop field the critical current diverges when $\varphi_{\mathrm{TL}}=90°$. The instability lines obtained for the FL are summarized in the current-field diagram in Fig. 2(a) by the green lines (FL unstable).

D. Critical currents for the SAF and the FL for $H_{\mathrm{app}}<0$

The calculations for the critical currents of negative applied fields and opposite FL direction are done in a similar manner. In the saturation and spin-flop regions the expressions of the critical currents are obtained by replacing $H_{\mathrm{app}} \rightarrow -H_{\mathrm{app}}$ in Eqs. (3) and (5) for the SAF and in Eqs. (8) and (9) for the FL. In these two cases, the sign of the critical current does not change. In the plateau region, Eq. (4) for the SAF is valid in the whole range of the plateau for both positive and negative fields. However, one has to consider that when the FL orientation switches, the expression in Eq. (4) and with this the critical currents change sign. In the case of the FL in the plateau region, one has to change the overall sign in Eq. (7) as well as the sign of H_{app} when the FL switches. Consequently, in negative field all three critical currents are positive for the SAF and negative for the FL.

The full diagram for positive and negative current and field is shown in Fig. 2(a), for the case of a slightly uncompensated SAF structure, for which the product $M_S d$ of the TL and BL are different [see figure caption of Fig. 1(a)]. For simplicity the FL switching is taken to occur at zero applied field and without hysteresis. As can be seen the diagram is not symmetric as a function of field in the spin-flop region. In positive field there is a divergence while in negative field, the divergence is absent. This is due to the asymmetric rotation of the TL for positive and negative fields, as discussed above in Sec. II A and shown in Fig. 1(b). In positive current φ_{TL} passes through 90° and the critical current diverges, while in negative current, φ_{TL} does not pass through 90° and no divergence occurs. Note also that this asymmetry vs field can be reversed when choosing material parameters or an AF exchange bias such that in positive (negative) applied fields the BL (TL) reverses and not the TL (BL) as in the case of Fig. 2(a). Finally, in the case of a compensated structure, φ_{TL} passes through 90° in both positive and negative fields and as a result the diagram is symmetric with respect to the applied field for $|H_{\mathrm{app}}|>|H_{\mathrm{SF}}|$, see Fig. 2(b).

It should also be pointed out here that the angular dependence of G has been neglected, so that in Fig. 2 there is no asymmetry for positive and negative currents (compare for instance the positive and negative critical currents of the FL in the plateau region).

As will be shown in Sec. III, these analytical calculations are a very good first approximation to obtain qualitatively the critical lines for a spin torque oscillator structure with a pinned SAF layer. However in order to investigate the nature and properties of the dynamics for currents above the threshold current, one needs to solve numerically the LLGS equation.

III. NUMERICAL CURRENT-FIELD DIAGRAM

A. Simulation details

In the numerical studies we have solved the LLGS equation Eq. (1) for the magnetizations of all three layers FL, TL, and BL simultaneously upon taking the following interactions into account. The BL is coupled via exchange bias to an antiferromagnet which is set into the positive X direction. For the coupling between the BL and TL an RKKY-type exchange interaction has been considered. The FL and TL are coupled via a mutual spin torque effect. This means that the instantaneous magnetization of the FL defines the polarizer direction for the TL and vice versa. Furthermore, the spin-polarization efficiencies η of Eq. (2) were chosen to be equal with $\eta_{\mathrm{FL}\rightarrow\mathrm{TL}}=\eta_{\mathrm{TL}\rightarrow\mathrm{FL}}=0.3$. As in the analytical discussion, the BL does not experience any spin torque. The demagnetizing field of all three layers has three components $\mathbf{H}_d=M_S(m_xN_x,m_yN_y,m_zN_z)$, where N_i are the demagnetizing factors due to the shape anisotropy of the considered layer calculated for rectangular nanopillars of 60×70 nm^2. The material parameters of all three layers used in the simulations are summarized in Table I. It is noted that although the TL and BL layer have different material parameters, the SAF structure is almost compensated (i.e., the product $M_S d$ is almost the same for both layers).

The macrospin solver for the three coupled LLGS equations is based on a predictor-corrector Heun scheme[29] using a time step of 1 fs. The applied field and injected current were modeled by step functions with a rise time of 2 ns. The total integration time varied from 100 up to 1000 ns according to the convergence speed of the solution for the three coupled layers toward the static or dynamic equilibrium state. Note that in contrast, a single layer LLGS solution converges to its equilibrium much faster in around 10–20 ns.

B. State diagram for a coupled system

The numerically calculated current-field diagram is shown in Fig. 3(a) for the material parameters given in Table I. The static and dynamic states are indicated by the dark and light gray regions, respectively. Here the field was swept at steps of 10 kA/m starting at zero field (FL and TL are antiparallel)

TABLE I. Parameters used in the numerical simulations. Here M_S is the saturation magnetization, K is a uniaxial magnetocrystalline anisotropy constant, d is the film thickness, N_x, N_y, and N_z are demagnetization factors, α is the damping constant, and H_{ex} is the exchange bias field that acts on the BL. The structure considered is almost compensated, i.e., the product $M_S d$ for the TL and BL are close with $(M_S d)_{TL}$=4020 μA and $(M_S d)_{BL}$=4000 μA.

	BL	TL	FL
M_s (kA/m)	1600	1340	1070
K (J/m^3)	8000	6700	5350
d (nm)	2.5	3.0	3.0
N_x	0.045	0.051	0.051
N_y	0.053	0.060	0.060
N_z	0.901	0.887	0.887
α	0.02	0.02	0.02
H_{ex} (kA/m)	40	0	0
η	0	0.3	0.3

and at a constant current-density value that was increased by 0.2×10^{12} A/m^2 for each field sweep. Comparison between Figs. 2(a) and 3(a) shows that the analytical approximate current-field diagram is in good qualitative agreement with the diagram calculated numerically for the three field regions. Here the spin-flop and saturation fields are indicated by the white horizontal dotted lines in Fig. 3(a). It is noted that for current amplitudes smaller than the critical current the spin-flop field and the saturation field under spin torque are not changed as compared to the zero current values. The quantitative differences between Figs. 2(a) and 3(a) are attributed to the fact that in the analytical calculations we have made the following simplifications. First, the instability conditions are investigated separately for the TL or FL without any coupling to the other layers. Second, in the spin-flop region a small out-of-plane component of TL or FL magnetization has been neglected (see Appendix B). Third, no angular dependence of the spin torque coefficients G has been considered in the analytical calculations. The more important differences in positive current and negative field range will be commented on in Sec. IV.

As a final point it is noted that in the diagram of Fig. 3(a) the boundaries of the light and dark gray regions separate static stable states from dynamic excitation states. These dynamic excitations of the coupled system can be either periodic steady state in-plane or out-of-plane oscillations or nonperiodic oscillations. These different dynamic states introduce further boundaries in the state diagram and will be addressed in the following sections where they will be compared to the dynamics of the uncoupled planar oscillator where only one layer is excited.

IV. PRECESSION TRAJECTORIES

A. Classification of stable trajectories

The numerical simulations reveal simultaneous excitations of the magnetization of all three layers for all field regions as well as for positive and negative currents. However the difference in amplitudes allows us to distinguish the current and field regions for dominant FL or SAF dynamics. These regions are indicated, respectively, by the green (FL) and red (SAF) lines in Fig. 3(a) and compare to the corresponding regions of the analytical diagram in Fig. 2(a).

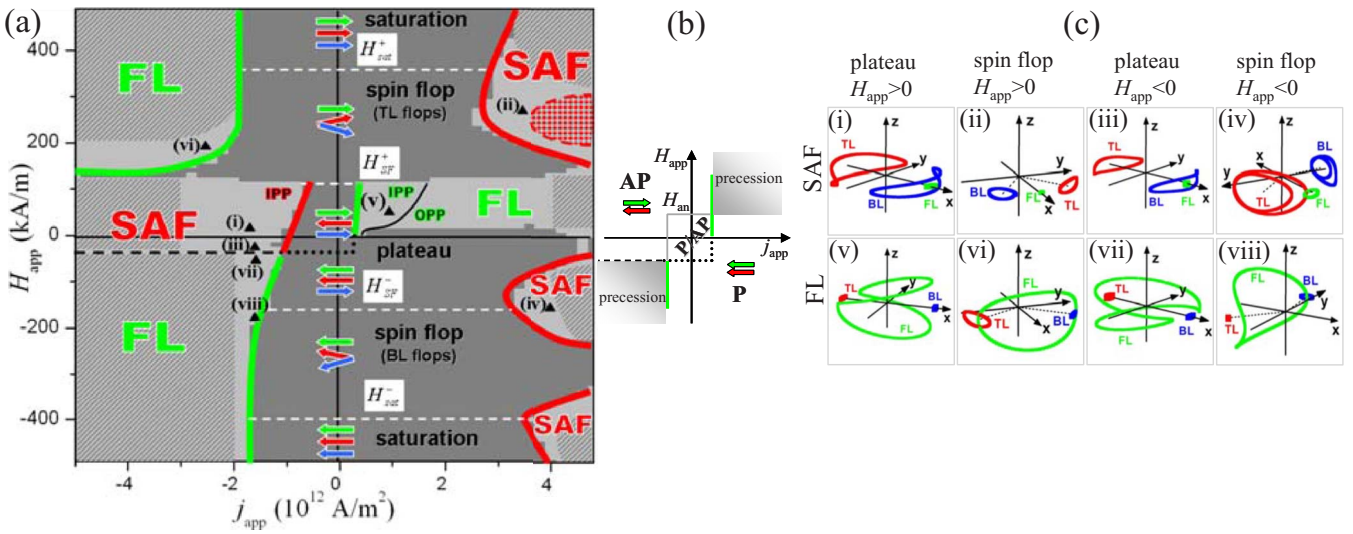

FIG. 3. (Color online) (a) Numerical current-field diagram. The layers' parameters used in the numerical simulations are summarized in Table I. The critical-field values calculated in the absence of an applied current are H^+_{sat}=358 kA/m, H^+_{SF}=112 kA/m, H^-_{SF}=−154 kA/m, and H^-_{sat}=−398 kA/m. (b) Schematical current-field diagram for an uncoupled spin torque oscillator with excitations in the FL only. Positive current corresponds to an electron flow from the polarizer (red arrow) to the free layer (green arrow). The black dashed and dotted lines as well as the green solid lines correspond qualitatively to those of the numerical diagram. (c) Typical trajectories plotted for several values of applied current and field corresponding to points (i)–(viii) in the diagram of (a) as indicated by the triangles. The blue/red/green colored trajectories correspond to the BL/TL/FL dynamics, respectively. Here H_{app} (kA/m) and j_{app} (10^{12} A/m^2) are (i) 20, −1.8, (ii) 280, 3.4, (iii) −20, −1.6, (iv) −150, 3.8, (v) 50, 1, (vi) 200, −2.4, (vii) −30, −1.6, and (viii) −190, −1.6.

For negative current and positive fields in the plateau region, as well as in positive current for positive fields above the spin-flop field, the SAF dominates the dynamics, with the oscillation amplitude of the FL magnetization being negligibly small in comparison to the SAF's amplitudes. Trajectories of these two regions are depicted in Fig. 3(c) (i) and Fig. 3(c) (ii), respectively, where it can be seen that the TL and BL perform large-angle coupled oscillations around their respective static equilibria. The corresponding clamshell-type trajectories are generally classified as in-plane precession (IPP).[6,21–23] It is noted that the excitations of the BL magnetization are not caused directly by the spin torque but are stimulated via the RKKY-exchange coupling to the oscillating TL. Furthermore it should be noted that even though the SAF is statically more rigid against field perturbation due to the strong RKKY coupling, it can be seen from Fig. 3(a) that the critical current required to induce stable periodic excitations might not be too different for the FL and the SAF. Thus, strong RKKY coupling strength does not mean absence of excitations. However with increasing RKKY coupling, the critical current increases [see Eq. (4)] and the precession amplitude reduces decreasing in the experiment the output signal.

For the opposite current sign of the plateau and spin-flop region, it is the FL magnetization amplitude which is much larger than the oscillation amplitudes of the SAF magnetization. The corresponding trajectories are depicted in Fig. 3(c) (v) and Fig. 3(c) (vi), where it can be seen that the FL magnetization performs IPP oscillations around its static equilibrium (along the positive X axis).

Finally, in negative current and for negative fields in the plateau region ($-H_{an} < H_{app} < H_{SF}^{+}$), it is the SAF that dominates at low-field values as shown in Fig. 3(c) (iii). It should be emphasized that this means in particular that in contrast to the FL dynamics, stable oscillations of the SAF's magnetization can be obtained in zero applied field, a point of interest for applications. However, when the field amplitude is larger than the FL anisotropy field $H_{app} < -H_{an}$ [dashed black line in Fig. 3(a)], the FL orientation switches and now the FL amplitude is larger [see Fig. 3(c) (vii)]. Here it is of interest to note that the static FL switching field at $H_{app} = -H_{an}$ extends into the dynamic region, separating sharply the FL and SAF dynamics.

B. Comparison to the uncoupled dynamics

With this the dynamics of the spin torque coupled FL-SAF system seems to be quite similar to the uncoupled case. Here uncoupled means that the spin torque is acting on the FL or the TL only, while in the coupled case the spin torque acts on the FL and TL simultaneously. For comparison a schematic current-field diagram of the uncoupled FL dynamics is shown in Fig. 3(b), where there is clear correspondence for the dynamics in negative current and negative field ($|H_{app}| < H_{an}$) for all three field regions of the SAF due to the dominant parallel alignment between the TL and the FL. The excitation region in positive field is split into excitations at positive current in the plateau region (antiparallel, AP, alignment between TL and FL) and excitations in negative current above the spin-flop field (parallel, P, alignment between TL and FL). Further correspondence exists in the plateau region for the dominant FL dynamics of the coupled system, where there is a clear transition from in-plane to out-of-plane (OPP) periodic oscillations.[6,21–23] The corresponding boundary is given in Fig. 3(a) by the solid black line. In contrast, for the SAF dynamics in the plateau region, no clear transition to OPP periodic oscillations could be established for the current values presented in the diagram due to the occurrence of unstable trajectories (see Sec. IV C).

C. Unstable trajectories and period-doubling bifurcation

1. Unstable trajectories

From the comparison presented in Sec. IV B one might conclude that the magnetization dynamics as well as the current-field diagram of the coupled system correspond more or less to those expected for the uncoupled case. However, there are some important consequences that result from the spin torque coupling between the FL and the SAF and the RKKY coupling within the SAF. Namely, well-defined periodic oscillations, such as shown in Fig. 3(c), are only obtained relatively close to the critical current, i.e., for current values and thus oscillation amplitudes that are not too large. For increasing current, but also for increasing field, it was difficult to establish periodic excitations even for relatively long integration times of 1000 ns. These nonperiodic solutions are furthermore independent of the time step used for integration, so we conclude that these nonperiodic solutions do not result from an instability of the integration scheme used. We rather attribute them to the magnetization dynamics of a nonlinear coupled system that can develop chaotic dynamics when there are more than two degrees of freedom.[30–32]

2. Period doubling

For the SAF dynamics in the spin-flop region (positive current and positive field), it was possible to follow a period-doubling route from fully periodic trajectories to nonperiodic trajectories as a function of increasing current amplitude. This is shown in Fig. 4 for a value of $H_{app} = 250$ kA/m. Following the suggestion of Ref. 32 to characterize such period doubling, we have plotted for a given time series the minimum values of the m_x component of the TL as a function of increasing current. For a purely one-period trajectory only one value exists, while for a double period oscillation, there are two well-defined minimum m_x values, etc. As seen in Fig. 4, there is clear period doubling when increasing the current from 3.0 to 4.2×10^{12} A/m^2. Above 4.2×10^{12} A/m^2 further period doubling occurs over very short current steps that are difficult to follow in the simulation.

3. State diagram

In the diagram of Fig. 3(a), the red hatched area in the spin-flop region (positive current) indicates qualitatively where period doubling to nonperiodic oscillations has been observed for the SAF. Such period doubling is reminiscent of a transition to chaotic dynamics. However, in order to estab-

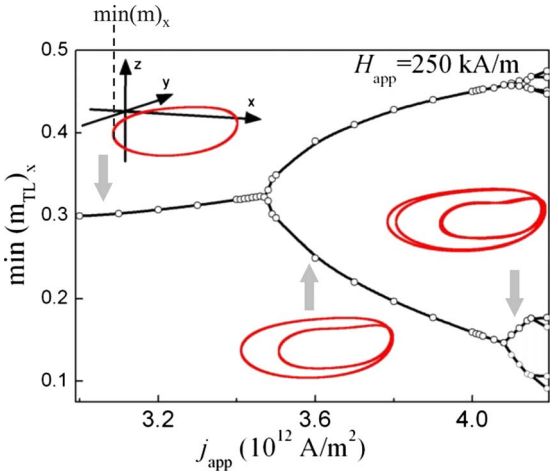

FIG. 4. (Color online) The minimum value of the m_x component of the TL for IPP oscillations as a function of increasing current amplitude in the spin-flop region. A clear period-doubling bifurcation from stable to unstable trajectories is observed.

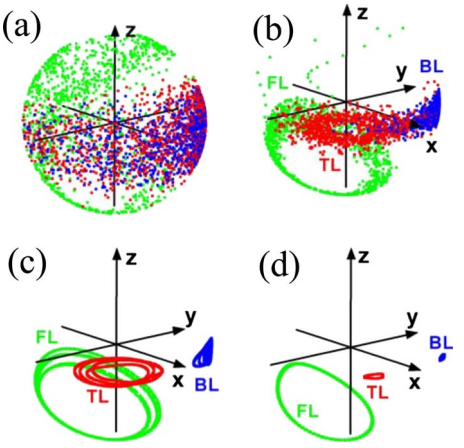

FIG. 5. (Color online) Trajectories for the FL (green), TL (red), and BL (blue) in the spin-flop region at negative current (H_{app} =300 kA/m, $j_{app}=-5\times10^{-12}$ A/m^2) for different values of the spin torque prefactor G_{TL} with (a) 0.3, (b) 0.25, (c) 0.2, and (d) 0.15. This variation of G_{TL} corresponds to an effective reduction of the spin-polarization efficiency η [see Eq. (2)] and thus an effective reduction of the spin torque that acts on the TL.

lish whether the observed unstable nonperiodic trajectories are indeed chaotic, more detailed analyses are required to establish, for example, the Lyapunov exponent, exact Poincaré maps, sensitivity to initial conditions, and possible attractor trajectories.[30–32] This is beyond the scope of this paper. We therefore content ourselves to indicate in the diagram of Fig. 3(a) by the gray hatched areas the field and current ranges where nonperiodic oscillations have been observed for the SAF and FL dominated dynamics. The boundaries should not be taken too literally and are only indicative. More detailed studies show that they can be rather ragged and zig-zag-like. In many cases, the transition to the nonperiodic oscillations cannot be followed as nicely as in Fig. 3(d), since here the current range of the transition is rather small. It is thus also not clear yet whether the same period-doubling bifurcation route is followed in all cases. This concerns in particular the SAF dominated dynamics in negative field and positive current [see Figs. 3(a) and 3(c)(iv)], which did not reveal a pronounced range of periodic oscillations and has therefore not been studied in further detail in this paper. The predominance of nonperiodic oscillations might be indirectly the reason why the critical boundaries in this region deviate most strongly from the simple analytical solutions, compare Fig. 2.

4. Dependence of unstable trajectories on the coupling

Two more points need to be mentioned here. The period-doubling route to unstable oscillations in the case of the SAF dynamics in the spin-flop region [see Fig. 4] is mainly due to the RKKY coupling between the TL and the BL and not due to the spin transfer coupling to the free layer. The same transition to nonperiodic dynamics is obtained for the SAF when setting the spin torque on the FL to zero (i.e., spin torque is only acting on the SAF and not on the FL). This shifts slightly the boundaries but does not eliminate the nonperiodic trajectories. An important question to address here in future studies will be the exact role of the RKKY coupling strength on the presence of unstable trajectories.

In contrast to this, the nonperiodic oscillations of the FL are a direct consequence of the spin torque coupling to the SAF. Since for these nonperiodic oscillations also the SAF amplitudes can be relatively large [see Figs. 5(a) and 5(b)], it is not clear whether the transition to nonperiodic oscillations is induced by the FL dynamics or induced indirectly by an unstable SAF dynamics. However, it is clear that upon reducing the spin torque coupling, i.e., the spin torque acting on the TL, the nonperiodic oscillations of the FL transform to stable periodic oscillations, where at the same time the amplitudes of the SAF magnetizations decrease. This is demonstrated in Fig. 5, where the FL and SAF trajectories are shown for negative current and positive field in the spin-flop region as a function of the relative spin torque that acts on the FL and TL. A further consequence here is that for the material parameters chosen for the diagram in Fig. 3(a), the transition of IPP to OPP oscillations in the spin-flop and saturation regions is masked by unstable trajectories. Reducing the coupling to the TL, OPP trajectories can be stabilized, as demonstrated by the example of Fig. 5(d).

5. Consequences for the experiments

An important consequence of nonperiodic oscillations will be the loss of coherence and thus broadened linewidths and reduced peak power of the microwave emission lines, leading finally to emission peaks that are lost in the background noise. Thus the spin torque coupling between the free layer and the pinned layer as well as the RKKY coupling within the SAF structure does provide a mechanism to explain loss of coherence at higher current and/or field values. We expect that other coupling mechanisms, such as dynamic dipolar coupling between the free and the pinned layers, will have similar effects.

V. FREQUENCY OF THE FL AND SAF EXCITATIONS

While at first sight the periodic IPP and OPP oscillations of the coupled FL-SAF dynamics reveal the basic features

known from the uncoupled FL dynamics[6,21–23] as long as the current is below the "nonperiodic" precession threshold, there are some marked differences concerning the frequency dependencies which are discussed in this section. In particular in the plateau region, which we will focus on, the SAF can have a substantial influence on the periodic FL dynamics (positive current) as compared to the uncoupled FL dynamics. Similarly, for the dominant SAF dynamics (negative current), where the TL is excited by spin transfer torque, the simultaneous excitation of the BL can lead to important changes in the frequency vs current dependence.

A. FL-IPP and FL-OPP dynamics in the plateau region at $j_{app}>0$ and $H_{app}>0$

1. Locking of the IPP modes

In the plateau region at low positive field and positive current amplitudes, an IPP-FL steady state oscillation is excited, where the FL amplitude dominates over the SAF amplitudes [see Fig. 3(c) (v)]. Here the frequency reveals a Kittel-type increase as a function of increasing applied bias field, as shown in Fig. 6(a) by the dots for $j_{app}=0.4$ and 0.6×10^{12} A/m^2. This dependence compares well to the frequencies of the uncoupled FL dynamics shown by the dashed lines in Fig. 6(a). However, for larger current amplitudes important changes occur. As can be seen from Fig. 6(a), for current values above $j_{app}=0.8\times10^{12}$ A/m^2, the frequency first increases with field, following the uncoupled dispersion and then reveals around 50 kA/m an abrupt upward frequency jump which can be as large as a few gigahertz. This jump is associated with a change in the slope from positive to negative and a relatively flat frequency-field dispersion. At larger fields, toward 100 kA/m, the frequency seems to recover the uncoupled f vs H_{app} dispersion curve. Above the spin-flop field $H_{SF}^{+}=112$ kA/m the FL dynamics vanishes.

It is noted that the field value at which the jump occurs increases slightly with increasing current and that it is well below the spin-flop field and therefore not associated to the spin flop. However, it can be related to the SAF dynamics which is excited due to the mutual spin torque between the FL and the TL-SAF. Namely, when looking closer at the FL and SAF trajectories, it is found that the FL precession amplitude reduces significantly at the jump while the amplitudes of the SAF layers increase [see Figs. 6(b), 6(c), and 6(e)]. This change in amplitudes is associated with an overall decrease in total energy (averaged over one precession period) [see Fig. 6(d)], for which the average free layer energy decreases while the average SAF energy increases slightly. At first sight, it might be surprising that an upward frequency jump is associated with a reduction in energy. However, this is a general feature of IPP oscillations well known from the uncoupled FL dynamics. This results from the negative nonlinear frequency shift coefficient[6,33] and expresses the fact that the frequency decreases upon increasing precession amplitude and thus upon increasing average precession energy.

The frequency jump is interpreted in the following way. The spin transfer torque acting on the TL magnetization stabilizes an antiparallel orientation between the TL magnetization with respect to the FL magnetization direction. On the other hand, due to the spin current-induced steady state IPP-FL oscillations, the varying FL magnetization orientation acts via the spin transfer torque as an external pumping for the TL magnetization, which is forced to periodically follow the FL motion in a nonresonant manner in order to maintain an antiparallel alignment. When the external pumping frequency (i.e., the IPP-FL steady state frequency) coincides with the SAF eigenmode frequency, resonance excitation of the SAF occurs. This results in an important increase of the SAF precession amplitude as shown in Figs. 6(c) and 6(e) and a strongly coupled oscillation between the FL and the SAF magnetizations, where the FL frequency seems to lock onto the SAF frequency which is close to its ferromagnetic resonance (FMR) frequency.

In order to substantiate this hypothesis we have plotted in Fig. 6(a) the FMR frequency-field dispersion of the SAF

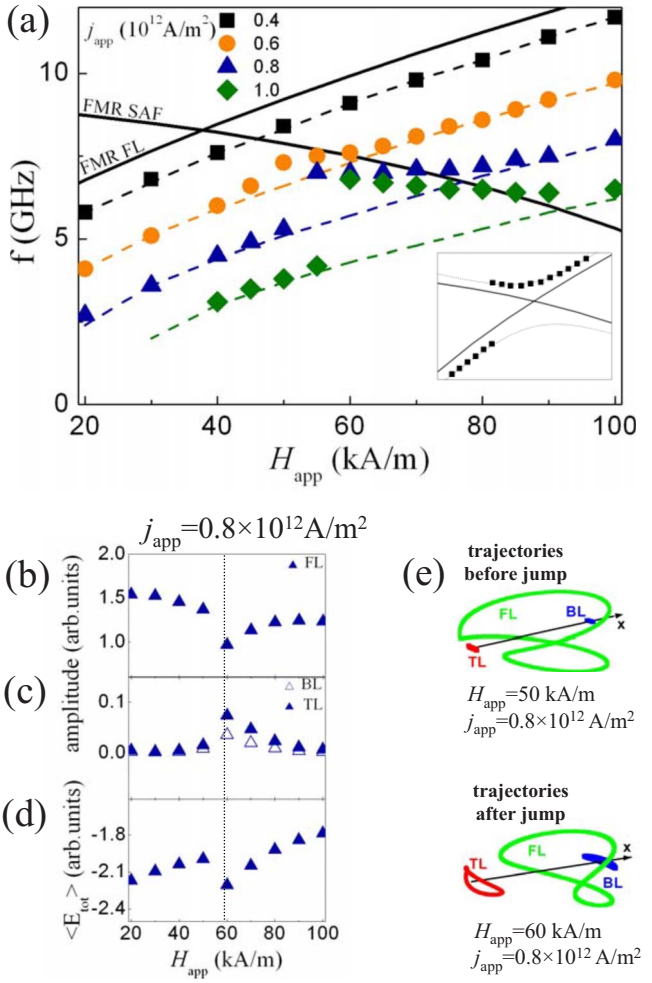

FIG. 6. (Color online) (a) IPP frequencies of the FL as a function of applied field. The dashed lines correspond to the frequency dependence calculated for the uncoupled FL excitations with fixed polarizer. The dark solid lines correspond to FMR-FL frequencies (f increasing with H_{app}) and FMR-SAF frequencies (f decreasing with H_{app}). Inset: Schematics of the mode repulsion for the FL frequency "locking" to the FMR-SAF frequency. (b) FL amplitude as a function of applied field. (c) BL and TL amplitudes as a function of applied field. (d) Average total energy as a function of applied field. (e) Dynamic trajectories of the FL/TL/BL before and after the frequency jump for field and current values as given on the figure.

which intersects the FL steady state dispersion of a given current at a field value that is close to the jump. The negative slope of the f vs H dispersion of the SAF is due to the fact that here the TL is antiparallel to the applied field [see lower branch in Fig. 1(c) in the plateau region and also Sec. V B]. In analogy to the mode crossing and mode repulsion in linear dynamics,[34] it seems that at the intersection of both dispersion curves, a splitting occurs which is schematically indicated in the inset of Fig. 6(a). Below the jump (upon increasing field) the system locks onto the FL dominated branch, but jumps onto the strongly coupled FL-SAF branch at some critical-field value due to the resonant excitation of the SAF. At higher field values the SAF goes off resonance again and the dynamics recovers the branch dominated by the FL dynamics. We note that this locking bears some resemblance to the spin transfer driven two-mode oscillator described in Ref. 35.

2. Locking of the OPP modes

This locking of the FL dynamics due to a resonant excitation of the SAF can also be clearly seen when plotting the frequency-current relation which is shown in Figs. 7(a) and 7(b) for both the IPP and OPP excitations of the coupled system (dots). For a field value for instance of 70 kA/m, the IPP-FL frequency first decreases for increasing current and then saturates at a value of 6.5 GHz [cf. also Fig. 6(a)]. For this field value, the OPP dynamics is not affected, where f increases with current. On the contrary, for lower field values such as 40 kA/m, a clear saturation of the OPP frequency can be seen over a relatively large current range [blue dots of Fig. 7(a)]. For comparison, the horizontal dashed lines in Fig. 7(a) give the SAF-FMR frequencies for the two field values which compare well to the frequency range where the IPP and OPP frequencies saturate. Although the actual locking frequency f_{lock} is lower than the pure SAF-FMR frequency, from the inset in Fig. 7(a) it can be seen that the locking frequency (dots) follows the SAF-FMR dependence (full line) decreasing with H_{app}. Thus, when the SAF-FMR frequency cuts the IPP or OPP branch, locking of the FL onto the SAF dynamics occurs over a given current range due to resonant excitation of the SAF. This locking range is hysteretic in current, as indicated in Fig. 7(a) for $H_{\mathrm{app}}=40$ kA/m, where it can be seen that upon increasing current (full dots) the FL dynamics remains locked to the SAF dynamics over a much larger range than upon decreasing current (open dots).

As in the case of the IPP locking shown in Figs. 6, 7(b), and 7(c) (right), the frequency locking of the OPP excitations is associated with a change in precession amplitudes and a reduction in the average total energy, as shown in Figs. 7(b) and 7(c) (left) for $H_{\mathrm{app}}=40$ kA/m. In the locking range, the total average energy of the OPP excitations saturates and makes an abrupt upward jump to higher values once the SAF goes off resonance at larger current [above 3×10^{12} A/m^2 in Fig. 7(c)]. Furthermore, in the locking range the SAF amplitudes strongly increase [see Fig. 7(b) (left)], while the FL amplitude of the OPP oscillation is reduced (not shown here), meaning that the OPP oscillation is characterized by a much reduced average out-of-plane m_z component [see Fig. 7(d) (left)]. When the SAF goes off resonance, the FL recovers its full amplitude, with a relatively strong m_z component. When this happens, the SAF amplitudes reduce [see Fig. 7(d) (right)], but more interestingly, the magnetizations of the TL and BL rotate in plane and away from the 0°/180° orientation. This rotation is similar to the rotation observed for a perpendicular polarizer,[36] where in the situation discussed here, the strong out-of-plane component of the FL-OPP mode acts almost like a perpendicular polarizer for the planar SAF.

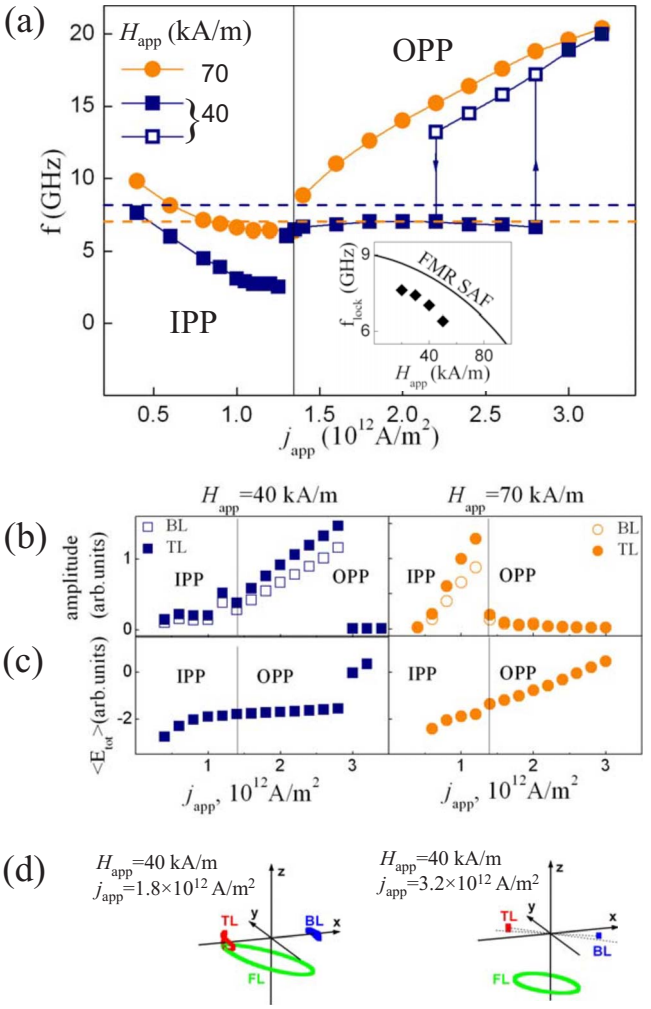

FIG. 7. (Color online) (a) IPP and OPP FL frequencies as a function of applied current in the plateau region. (b) BL and TL amplitudes vs current. (c) FL average energy vs current. (d) Typical FL OPP trajectories for low- and high-frequency modes. Inset in (a) shows the locking frequency f_{lock} in comparison to the SAF-FMR frequency.

3. Hysteresis

The occurrence of a hysteresis in Fig. 7(a) deserves a few comments. Hysteretic behavior between a static and a dynamic state has been found theoretically[36] and experimentally.[37] Another theoretical description[38] treats the hysteresis between a localized and extended spin-wave mode of a nanocontact, where for increasing current the system remains "blocked" in the extended mode, while for decreas-

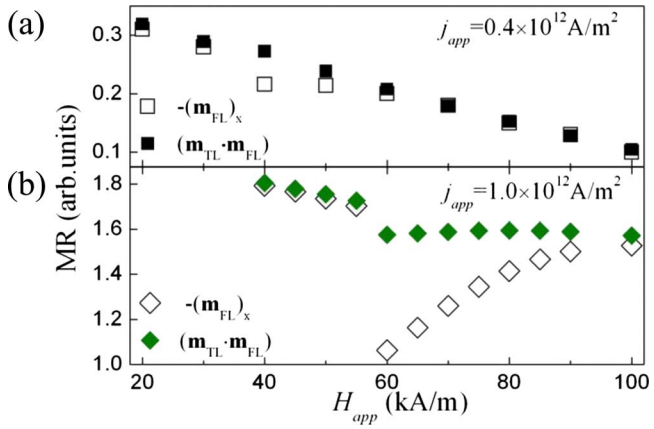

FIG. 8. (Color online) The calculated MR value as a function of applied field, estimated using either the projection of the free layer magnetization on the X axis (open dots) or the scalar product between the free layer and top layer magnetization ($\mathbf{m}_{FL}\cdot\mathbf{m}_{TL}$) (full dots): (a) for low current without frequency locking and (b) for larger current with frequency locking [cf. Fig. 6(a)].

ing current the localized mode prevails, which is considered as the actual eigenmode for the given external conditions (field, current). In this context the hysteresis between the FL-SAF coupled oscillation and the FL dominated oscillation can be considered similar, where the coupled mode is blocked in a low energy state upon increasing current even though the frequencies of the FL and the FMR-SAF modes are quite different. A relatively large current is required for the system to transit from the FL-SAF coupled oscillation to the uncoupled FL oscillation. Upon decreasing the current again, the current value has to be decreased beyond the value of this transition before the FL will lock onto the SAF-FMR excitation, most likely since the uncoupled FL oscillation is the actual eigenmode in this given current range.

4. Output signal

As a final point on the coupled IPP-FL dynamics we want to make the following comment which is relevant for experiments. The output signal measured on a spectrum analyzer is usually considered to be proportional to the FL precession amplitude projected on a fixed reference axis. For the uncoupled case, this is the pinned SAF-TL orientation, which is along the negative X axis in the plateau region (see Fig. 1). Outside the FL locking range, this is a good approximation, as shown in Fig. 8(a) where the amplitude of the m_x component (full squares) is given as a function of the applied field for a low current value of $j_{app}=0.4\times10^{12}$ A/m^2. In this case, the magnetoresistance (MR) signal decreases with field, since a stronger field stiffens the motion and thus reduces the precession amplitude of the IPP mode. For a current value of 1.0×10^{12} A/m^2, the projection onto the X axis, i.e., the m_x component, also first decreases, but shows a strong downward jump when the SAF resonance sets in [cf. Figs. 6(b) and 6(d). However, due to the increased oscillation amplitude of the TL, the projection onto the X axis is not the relevant parameter for the measured MR signal. Instead one has to consider the scalar product of the FL and TL magnetizations ($\mathbf{m}_{TL}\cdot\mathbf{m}_{FL}$). As can be seen in Fig. 8(b), this scalar product is much larger than the projection onto the X axis since both the FL and the TL have relatively large oscillation amplitudes that are out of phase. Thus due to the TL oscillation, the total MR signal is enhanced and as a result the total jump in the output signal is much smaller. In consequence the overall change in amplitude remains moderate despite the strong actual change in the FL precession amplitude. This example shows that one has to be careful when trying to extract the FL precession amplitude from the measured output signal.

5. Conclusion

To conclude on this section of the FL dynamics in the plateau region for positive current and positive field, one can say that the mutual spin torque interaction between the FL and the TL leads in a given field and current range to a resonant excitation of the SAF which results in a locking of the FL frequency onto the SAF-FMR frequency. This is a clear manifestation that the mutual spin torque interaction plays a role for the FL dynamics. Quite generally such a dynamic interaction due to spin torque but also any other dynamic interaction (e.g., dipolar coupling) might provide a mechanism for observed frequency jumps in experiments[8,9,11,39,40] that have not been explained satisfactorily in a number of cases. Furthermore, in the locking range for the strongly coupled oscillations, the measured output signal can no more be related in a simple way to the FL precession amplitude, since here the signal is given by the scalar product of the FL and TL motions.

B. SAF dynamics at $j_{app}<0$ in the plateau region

1. SAF trajectories

At negative current and for fields in the plateau region ($-H_{an}<H_{app}<H_{SF}$) the SAF dominates the dynamics of the periodic oscillations [cf. diagram in Fig. 3(a)]. Here the BL and TL oscillate around, correspondingly, the positive and negative X-axis directions. This is an acoustic-type oscillation, where along one oscillation period the magnetizations of both layers are "in phase" along the Z direction, meaning that they have the same sign when they reach the maximum out-of-plane excursion. In contrast to this, for the in-plane excursion they are "out of phase," meaning that they have opposite signs in the Y direction. This is due to the RKKY coupling, which tries to keep the TL and BL antiparallel along the precession trajectory.

2. Locking of the SAF dynamics

The frequency-field dispersion values are shown in Fig. 9(a) for different current values. As can be seen, the field dependence follows the FMR relation with a frequency downshift upon increasing field. This decrease is due to the fact that here the low-frequency SAF branch is observed, compare acoustic branch in Fig. 1(c), for which the antiparallel alignment of the TL with respect to the applied field determines the frequency. Since here the applied field op-

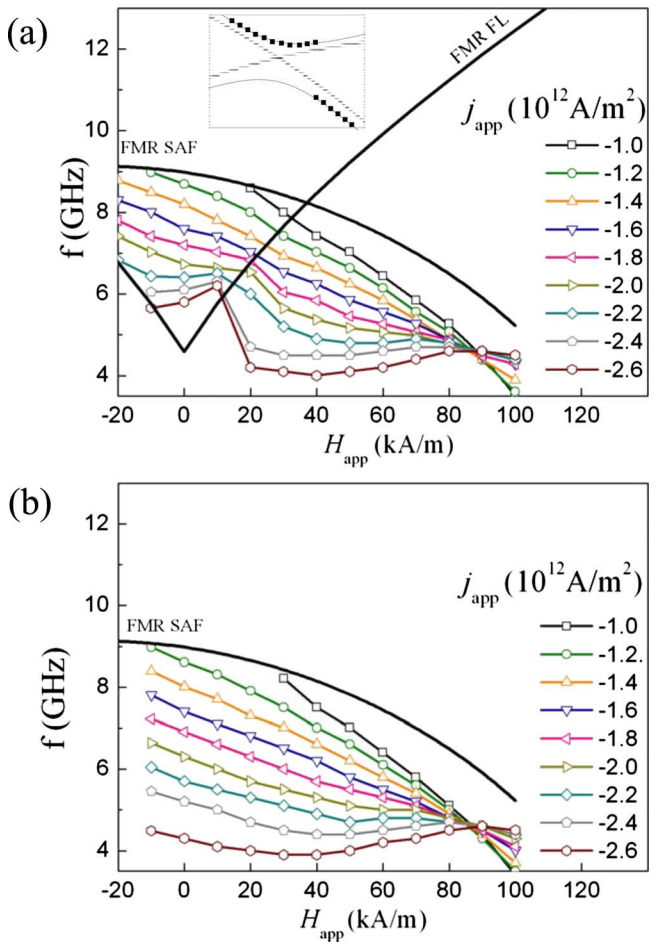

FIG. 9. (Color online) IPP frequency vs applied field for the dominant SAF excitations in the plateau region and for different values of the applied current as indicated on the figures for (a) the spin torque coupled system and (b) for the uncoupled SAF oscillations. The dark solid lines correspond to the FMR-FL and the FMR-SAF frequencies. Inset in (a): Schematics of the mode repulsion for the SAF frequency "locking" to the FMR-FL frequency.

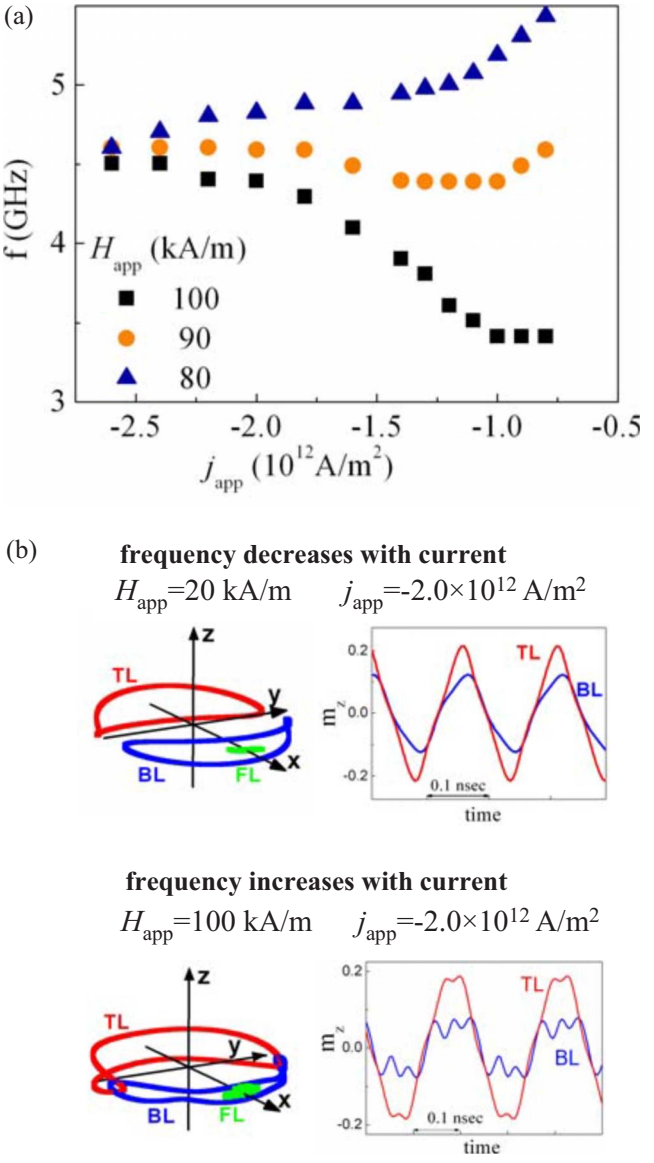

FIG. 10. (Color online) (a) IPP frequencies as a function of applied current for the dominant SAF excitations in the plateau region and for three different values of the applied field as indicated on the figure. (b) Typical trajectories and time evolution of the m_z component of the BL and TL magnetization for the spin torque driven IPP trajectories in the frequency redshift regime (upper panel) and in the frequency blueshift regime (lower panel).

poses the internal field, the frequency goes "soft" (i.e., to zero) at the spin-flop field.

Similarly to the abrupt jumps observed for the FL dominated steady state oscillations in Fig. 6(a), the SAF dominated oscillations also show at larger current values an abrupt jump of a few gigahertz, which in this case is shifted downward. This downward jump is explained in analogy as a resonance excitation of the "polarizing" FL, where the SAF excitations lock over a small field range onto the FL-FMR dynamics [see inset in Fig. 9(a)]. The corresponding FL-FMR dispersion is shown in Fig. 9(a), where it can be seen that the jumps occur at the crossing of the FL-FMR frequencies with the SAF excitation frequencies. Note that the jumps are absent for the uncoupled SAF dynamics (no spin torque on the FL), as shown in Fig. 9(b).

3. Blueshift of IPP modes

Besides the resonant excitation of the FL induced by the SAF steady state oscillations, there is another noticeable feature that is independent of the coupling between the TL and the FL. From Figs. 9(a) and 9(b) it can be seen that for increasing field, the frequencies at different current values cross more or less around H_{app}=90 kA/m. As a consequence, while at low fields the frequency as a function of current is shifted to lower frequencies (redshift) as expected for IPP oscillations, it is shifted to higher frequencies (blueshift) for fields above 90 kA/m [see Fig. 10(a)]. The fact that this occurs for the coupled and uncoupled SAF dynamics [see Figs. 9(a) and 9(b)] means that this crossover is an intrinsic feature of the spin transfer driven large amplitude SAF dynamics and not an effect of the mutual spin torque coupling. Interestingly this crossing and change from red-

shift to blueshift have recently been observed in our experiments.[20]

In order to explain this we would like to note the following. Contrary to the field dependence of the FL, in the case of the SAF the applied field counteracts the RKKY coupling and thus reduces the effective internal field for the TL. This results in a decrease of the precession frequency as a function of increasing applied field, accompanied by an increase in precession amplitude as is typical for IPP trajectories. Similarly, upon increasing the current at low or zero-bias field, the precession amplitude increases, resulting in a decrease in frequency. Upon increasing both field and current, which both act so as to increase the precession amplitude, there seems to exist an upper limit of the precession amplitude imposed by the RKKY coupling. This is shown by the comparison of the two trajectories in Fig. 10(b) for low and large field values at $j_{\mathrm{app}}=-2\times10^{12}$ A/m^2. In Fig. 10(b) this is more quantified by plotting the time evolution of the m_z component. While for low field (current) the m_z component is more or less sinusoidal, at larger field the m_z component is reduced, which leads to a "flattened" trajectory. This reduction in the m_z component is attributed to the following. As indicated above, the TL and BL are in-phase along the Z direction. For large precession amplitudes the TL and BL magnetizations come thus relatively close at their respective maximum m_z value. This results in a relatively strong RKKY interaction energy. In order to minimize this energy, the m_z component does not fully develop and the trajectory flattens. In addition, the BL develops some modulation of the m_z component [see Fig. 10(b)]. One might suggest that the flattened m_z component reduces the total length of the precession trajectory which in turn results in an increase of the precession frequency. Thus the precise balance between the different torques acting along the precession trajectory of a large amplitude SAF oscillation results in a gradual change from redshift to blueshift of the frequency vs current or equivalently to the crossing of the f vs H_{app} dispersions shown in Fig. 9.

C. Dynamics outside the plateau region

In this section, we summarize briefly the frequency dependence of other parts of the current-field diagram. As already described in Sec. IV, the spin-flop region and the saturation region are characterized by large areas of nonperiodic trajectories, so that the dynamics cannot be followed over large current or field values for the simulation parameters chosen here. It is only noted here that at positive field in the spin-flop region the frequency vs current amplitude decreases as expected for an IPP oscillation. This is true for the SAF dominated ($j_{\mathrm{app}}>0$) and FL dominated ($j_{\mathrm{app}}<0$) oscillations. The f vs j_{app} dispersion is indicated in the inset of Fig. 11(b) for the SAF case. Another point of interest for the SAF dominated oscillations is that the frequency vs field follows the FMR dispersion, as shown in Fig. 11 [cf. Fig. 1(c)] across the spin-flop and saturation regions. However, the applied field where the frequency goes to zero appears to be shifted to lower values as compared to the saturation field.

Following the FL dynamics in negative field and negative current reveals only in the plateau region typical IPP behavior with a f vs H_{app} dependence that is Kittel type (f increasing with H_{app}, but lower than the FMR frequency) and frequency redshift vs current. Following this excitation into the spin flop or saturation region was difficult due to the development of nonperiodic oscillations.

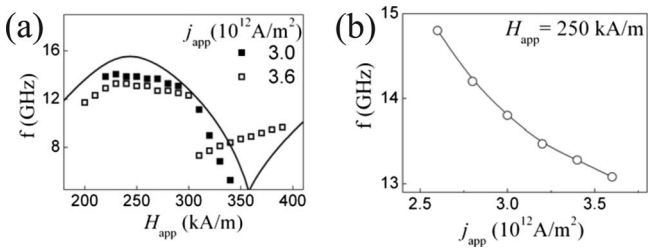

FIG. 11. (a) SAF IPP frequencies for applied fields in the spin-flop region and the saturation region for two different values of the applied current as indicated on the figure. (b) SAF IPP frequencies as a function of the applied current for a field value that corresponds to the spin-flop region.

VI. SUMMARY

In this paper we have discussed the spin-polarized current driven microwave excitations for a coupled magnetic layer system that consists of a free layer and an RKKY coupled synthetic antiferromagnetic pinned layer. Due to spin transfer torque both the free layer and the SAF pinned layer can be excited. For this system we first have derived the state diagram analytically as well as by numerical solution in a macrospin approach. The shape of the diagram bears resemblance to the uncoupled free layer dynamics and its modifications are closely linked to the reorientation of the SAF layers magnetization as a function of applied field throughout the spin-flop and saturation regions. While all three magnetic layers are excited simultaneously once the current is larger than a critical current, dominant free layer or SAF excitations can be identified in given current and field regions. For low current values close to the critical current, the dynamic states are stable periodic oscillations. For larger current amplitudes unstable (nonperiodic) oscillations do exist. In special situations a clear period-doubling route from stable to unstable trajectories was identified. Such unstable trajectories are a consequence of the RKKY and/or spin torque coupling and do not appear for a single magnetic layer. They are a likely source of linewidth broadening in the experiment and vanishing of microwave emission peaks under large currents. Another clear consequence of the mutual spin torque interaction between the free layer and the SAF pinned is the locking of the current-induced steady state excitations of one layer onto the FMR frequencies of the other layer. This occurs whenever the FMR frequency dispersion (as a function of current or field) of for instance the SAF crosses the frequency dispersion of the large-angle current driven excitations of the free layer (and vice versa). At this crossing jumps in the frequency dispersion occur and the frequency evolution resembles the mode repulsion of linear spin-wave dynamics. We note that we believe that these two effects (nonperiodic trajectories and frequency locking) are

not particular to the mutual spin torque interaction but should also be observed for other types of dynamic interactions such as dipolar coupling. Finally, for the spin current driven excitations of the SAF layers a clear difference as compared to the FL dynamics has been found in the plateau field region. This difference is independent of the mutual spin torque coupling between the FL and the SAF and is thus attributed to the large-angle current driven dynamics of the SAF structure. As in the case of a single free layer, at low field an IPP is excited where the TL and BL precess around their respective static in-plane equilibrium position. For low applied fields the frequency decreases (redshift) upon increasing current as is typical for IPP modes. However, upon increasing applied field, the frequency redshift of the IPP mode goes over into a frequency blueshift (frequency increases with current), while the precession character of the IPP mode does not change. We attribute this to the RKKY coupling between the TL and BL of the SAF that reduces the out-of-plane magnetization component of the IPP trajectories and thus increases the precession frequency. While the latter effect has recently been observed in our experiments, it will be of interest to also confirm the frequency locking due to mutual spin torque (or dynamic dipolar) interaction. Finally it is noted that in the simulations so far only the equivalent of the low-frequency acoustic branch [see Fig. 1(a)] has been found.

ACKNOWLEDGMENTS

We acknowledge support from the French National Research Agency under the programs CARNOT and PNANO/MagICO (Contract No. ANR-05-NANO-044) as well as the French program ANVAR.

APPENDIX A

1. Energy density of the SAF

Consider two ferromagnetic layers with normalized magnetization vectors $\mathbf{m}_{\mathrm{BL}}$ and $\mathbf{m}_{\mathrm{TL}}$ coupled antiferromagnetically via the nonmagnetic spacer. Both layers have uniaxial anisotropy and the $\mathbf{m}_{\mathrm{BL}}$ is exchanged biased by an antiferromagnet. The equilibrium configuration is determined by minimizing the total free energy per unit area σ. In our case the energy per unit area is written as a sum of Zeeman (applied field H_{app}), anisotropy, demagnetizing, exchange bias, and RKKY energy terms (for notations, see the text)

$$\sigma = \sigma_{\mathrm{Zeem}} + \sigma_{\mathrm{an}} + \sigma_d + \sigma_{\mathrm{ex}} + \sigma_{\mathrm{RKKY}},$$

where

$$\sigma_{\mathrm{Zeem}} = -\mu_0 M_{S(\mathrm{BL})} d_{\mathrm{BL}} m_{x(\mathrm{BL})} H_{app} - \mu_0 M_{S(\mathrm{TL})} d_{\mathrm{TL}} m_{x(\mathrm{TL})} H_{\mathrm{app}},$$

$$\sigma_{\mathrm{an}} = \mathrm{const} - K_{\mathrm{BL}} d_{\mathrm{BL}} m_{x(\mathrm{BL})}^2 - K_{\mathrm{TL}} d_{\mathrm{TL}} m_{x(\mathrm{TL})}^2,$$

$$\sigma_d = 0.5\mu_0 M_{S(\mathrm{BL})}^2 d_{\mathrm{BL}} \mathbf{m}_{\mathrm{BL}} \hat{N}_{\mathrm{BL}} \mathbf{m}_{\mathrm{BL}} + 0.5\mu_0 M_{S(\mathrm{TL})}^2 d_{\mathrm{TL}} \mathbf{m}_{\mathrm{TL}} \hat{N}_{\mathrm{TL}} \mathbf{m}_{\mathrm{TL}},$$

$$\sigma_{\mathrm{ex}} = -\mu_0 M_{S(\mathrm{BL})} d_{\mathrm{BL}} m_{x(\mathrm{BL})} H_{\mathrm{ex}},$$

$$\sigma_{\mathrm{RKKY}} = -J_{\mathrm{RKKY}} \mathbf{m}_{\mathrm{BL}} \mathbf{m}_{\mathrm{TL}}.$$

Here K_{BL} and K_{TL} are the uniaxial magnetocrystalline anisotropy constants of the BL and TL, respectively. In our calculations the anisotropy constant represents a small magnetocrystalline anisotropy and the shape anisotropy which is taken into account explicitly via the shape demagnetization factors. Thus the total anisotropy constant is given by

$$B_{\mathrm{BL,TL}} = K_{\mathrm{BL,TL}} - \frac{\mu_0 M_{S(\mathrm{BL,TL})}^2}{2}[N_{x(\mathrm{BL,TL})} - N_{y(\mathrm{BL,TL})}],$$

and the corresponding in-plane anisotropy fields are given by $H_{\mathrm{an}} = 2B/(\mu_0 M_S)$ with N_x and N_y the in-plane demagnetizing factors. The out-of-plane demagnetizing fields are given by $H_d = M_S N_z$, with N_z out-of-plane demagnetizing factor.

The RKKY coupling field is defined as $H_{\mathrm{RKKY}} = |J_{\mathrm{RKKY}}|/\mu_0 M_{S(\mathrm{TL})} d_{\mathrm{TL}}$.

2. Spin-flop and saturation fields

At zero applied current, $\mathbf{m}_{\mathrm{BL}}$ and $\mathbf{m}_{\mathrm{TL}}$ stay in plane. The zero current expressions for the spin-flop and saturation critical fields are

$$\begin{aligned} H_{\mathrm{SF}}^{\pm} = {} & \frac{1}{2\mu_0^2 M_{S(\mathrm{BL})} M_{S(\mathrm{TL})} d_{\mathrm{BL}} d_{\mathrm{TL}}} (\mu_0 |J_{\mathrm{RKKY}}| [M_{S(\mathrm{BL})} d_{\mathrm{BL}} \\ & - M_{S(\mathrm{TL})} d_{\mathrm{TL}}] + d_{\mathrm{BL}} d_{\mathrm{TL}} \{2\mu_0 [B_{\mathrm{TL}} M_{S(\mathrm{BL})} - B_{\mathrm{BL}} M_{S(\mathrm{TL})}] \\ & - H_{\mathrm{ex}} \mu_0^2 M_{S(\mathrm{BL})} M_{S(\mathrm{TL})}\} \pm (J_{\mathrm{RKKY}}^2 \mu_0^2 [M_{S(\mathrm{BL})} d_{\mathrm{BL}} \\ & - M_{S(\mathrm{TL})} d_{\mathrm{TL}}]^2 + \mu_0^2 d_{\mathrm{BL}}^2 d_{\mathrm{TL}}^2 \{2[B_{\mathrm{BL}} M_{S(\mathrm{TL})} + B_{\mathrm{TL}} M_{S(\mathrm{BL})}] \\ & + H_{\mathrm{ex}} \mu_0 M_{S(\mathrm{BL})} M_{S(\mathrm{TL})}\}^2 \\ & + 2|J_{\mathrm{RKKY}}| \mu_0^2 d_{\mathrm{BL}} d_{\mathrm{TL}} [M_{S(\mathrm{BL})} d_{\mathrm{BL}} + M_{S(\mathrm{TL})} d_{\mathrm{TL}}] \\ & \times \{2[B_{\mathrm{BL}} M_{S(\mathrm{TL})} + B_{\mathrm{TL}} M_{S(\mathrm{BL})}] \\ & + H_{\mathrm{ex}} \mu_0 M_{S(\mathrm{BL})} M_{S(\mathrm{TL})}\})^{1/2}), \end{aligned} \tag{A1}$$

$$\begin{aligned} H_{\mathrm{sat}}^{\pm} = {} & \pm \frac{1}{2\mu_0^2 M_{S(\mathrm{BL})} M_{S(\mathrm{TL})} d_{\mathrm{BL}} d_{\mathrm{TL}}} (\mu_0 |J_{\mathrm{RKKY}}| [M_{S(\mathrm{BL})} d_{\mathrm{BL}} \\ & + M_{S(\mathrm{TL})} d_{\mathrm{TL}}] - d_{\mathrm{BL}} d_{\mathrm{TL}} \{2\mu_0 [B_{\mathrm{TL}} M_{S(\mathrm{BL})} \\ & + B_{\mathrm{BL}} M_{S(\mathrm{TL})}] \pm H_{\mathrm{ex}} \mu_0^2 M_{S(\mathrm{BL})} M_{S(\mathrm{TL})} \\ & + (J_{\mathrm{RKKY}}^2 \mu_0^2 [M_{S(\mathrm{BL})} d_{\mathrm{BL}} + M_{S(\mathrm{TL})} d_{\mathrm{TL}}]^2 \\ & + \mu_0^2 d_{\mathrm{BL}}^2 d_{\mathrm{TL}}^2 \{2[B_{\mathrm{BL}} M_{S(\mathrm{TL})} \\ & - B_{\mathrm{TL}} M_{S(\mathrm{BL})}] \pm H_{\mathrm{ex}} \mu_0 M_{S(\mathrm{BL})} M_{S(\mathrm{TL})}\}^2 \\ & + 2|J_{\mathrm{RKKY}}| \mu_0^2 d_{\mathrm{BL}} d_{\mathrm{TL}} [M_{S(\mathrm{BL})} d_{\mathrm{BL}} - M_{S(\mathrm{TL})} d_{TL}] \\ & \times \{2[B_{\mathrm{BL}} M_{S(\mathrm{TL})} \\ & - B_{\mathrm{TL}} M_{S(\mathrm{BL})}] \pm H_{\mathrm{ex}} \mu_0 M_{S(\mathrm{BL})} M_{S(\mathrm{TL})}\})^{1/2}). \end{aligned} \tag{A2}$$

APPENDIX B: LINEARIZATION OF LLGS FOR TL OF SAF IN THE LOCAL COORDINATE SYSTEM (X′,Y′,Z)

For positive applied field and the case of parallel alignment of the FL magnetization with the X axis the transverse components m_y' and m_z' are given to first order (neglecting terms in α^2) by

$$\frac{dm_y'}{dt} = (-1)^{n+1}\gamma m_z'\{H_d + [H_{\rm app} + (-1)^n H_{\rm an}]\cos\varphi_{\rm TL} - H_{\rm RKKY}\cos(\varphi_{\rm TL}+\varphi_{\rm BL})\} + \alpha(-1)^{n+1}\frac{dm_z'}{dt} + (-1)^n\gamma j_{\rm app}G(\eta,\theta)m_y'\cos\varphi_{\rm TL} + f_1,$$

$$\frac{dm_z'}{dt} = (-1)^n\gamma\{m_y'\cos\varphi_{\rm TL}[H_{\rm app} + (-1)^n H_{\rm an}] - m_y' H_{\rm RKKY}\cos(\varphi_{\rm TL}+\varphi_{\rm BL})\} + \alpha(-1)^n\frac{dm_y'}{dt} + (-1)^n\gamma j_{\rm app}G(\eta,\theta)m_z'\cos\varphi_{\rm TL} + f_2. \quad \text{(B1)}$$

Here, $|m_x'|=1$ and $n=0$ when m_x' is parallel to the X' axis while $n=1$ when m_x' is antiparallel to the X' axis.

The free terms

$$f_1 = -\gamma j_{\rm app}G(\eta,\theta)\sin\varphi_{\rm TL}$$

and

$$f_2 = (-1)^{n+1}\{\sin\varphi_{\rm TL}[H_{\rm app} + (-1)^n H_{\rm an}] - H_{\rm RKKY}\sin(\varphi_{\rm TL}+\varphi_{\rm BL})\}$$

do not depend on m_y' or m_z'.

For three field regions the initial conditions read $n=0$, $\varphi_{\rm TL}=0$, $\varphi_{\rm BL}=0$, $X=X'$, $Y=Y'$, $\mathbf{p}=(1,0,0)$ for saturation region, $n=1$, $\varphi_{\rm TL}=\pi$, $\varphi_{\rm BL}=0$, $X=X'$, $Y=Y'$, $\mathbf{p}=(1,0,0)$ for plateau region, and $n=0$, $\mathbf{p}=(\cos\varphi_{\rm TL},\sin\varphi_{\rm TL},0)$ for spin-flop region.

The linearization of LLGS is exact for the case of small (or close to π) in-plane angles between $\mathbf{m}$ and $\mathbf{p}$, as in the plateau and the saturation regions. In contrast, in the spin-flop region the noncollinear angles between $\mathbf{m}$ and $\mathbf{p}$ result in a small out-of-plane component for the TL magnetization which is neglected in the analytical estimation of the stability (Sec. II). Numerical integration of LLGS confirms that the out-of-plane component of any layers magnetization $|m_z|$ does not exceed 0.02 for applied currents below the threshold current.

APPENDIX C

Coefficients of the critical current [Eq. (6)] for the compensated case

$$a = \frac{K_{\rm TL}d_{\rm TL}}{|J_{\rm RKKY}| - K_{\rm TL}d_{\rm TL}},$$

$$b = \frac{2K_{\rm TL}}{\mu_0 M_{S({\rm TL})}},$$

$$c = \frac{(|J_{\rm RKKY}| - K_{\rm TL}d_{\rm TL})(\mu_0 M_{S({\rm TL})}^2 d_{\rm TL} + 2|J_{\rm RKKY}|)}{\mu_0^2 M_{S({\rm TL})}^2 d_{\rm TL}^2}.$$

*Corresponding author: dariamessage@yandex.ru
†Present address: CPMOH, Université Bordeaux 1, CNRS-UMR 5798, 33405 Talence, France.

[1] J. C. Slonczewski, J. Magn. Magn. Mater. **159**, L1 (1996); J. C. Slonczewski, J. Magn. Magn. Mater. **195**, 261 (1999).
[2] L. Berger, Phys. Rev. B **54**, 9353 (1996).
[3] J. A. Katine, F. J. Albert, R. A. Buhrman, E. B. Myers, and D. C. Ralph, Phys. Rev. Lett. **84**, 3149 (2000).
[4] J. Grollier, V. Cros, A. Hamzic, J. M. George, H. Jaffrès, A. Fert, G. Faini, J. B. Youssef, and H. Legall, Appl. Phys. Lett. **78**, 3663 (2001).
[5] J. C. Slonczewski, U.S. Patent No. 5695864 (9 December 1997).
[6] S. I. Kiselev, J. C. Sankey, I. N. Krivorotov, N. C. Emley, R. J. Schoelkopf, R. A. Buhrman, and D. C. Ralph, Nature (London) **425**, 380 (2003).
[7] W. H. Rippard, M. R. Pufall, S. Kaka, S. E. Russek, and T. J. Silva, Phys. Rev. Lett. **92**, 027201 (2004).
[8] S. I. Kiselev, J. C. Sankey, I. N. Krivorotov, N. C. Emley, M. Rinkoski, C. Perez, R. A. Buhrman, and D. C. Ralph, Phys. Rev. Lett. **93**, 036601 (2004).
[9] S. I. Kiselev, J. C. Sankey, I. N. Krivorotov, N. C. Emley, A. G. F. Garcia, R. A. Buhrman, and D. C. Ralph, Phys. Rev. B **72**, 064430 (2005).
[10] W. H. Rippard, M. R. Pufall, S. Kaka, T. J. Silva, and S. E. Russek, Phys. Rev. B **70**, 100406(R) (2004).
[11] I. N. Krivorotov, N. C. Emley, J. C. Sankey, S. I. Kiselev, D. C. Ralph, and R. A. Buhrman, Science **307**, 228 (2005).
[12] S. S. P. Parkin, N. More, and K. P. Roche, Phys. Rev. Lett. **64**, 2304 (1990); J. Unguris, R. J. Celotta, and D. T. Pierce, J. Appl. Phys. **75**, 6437 (1994); P. Bruno, J. Phys. Condens. Matter **11**, 9403 (1999).
[13] Q. Mistral, J.-V. Kim, T. Devolder, P. Crozat, C. Chappert, J. A. Katine, M. J. Carey, and K. Ito, Appl. Phys. Lett. **88**, 192507 (2006).
[14] A. Deac, K. J. Lee, Y. Liu, O. Redon, M. Li, P. Wang, J. P. Nozières, and B. Dieny, Phys. Rev. B **73**, 064414 (2006).
[15] A. V. Nazarov, K. Nikolaev, Zh. Gao, H. Cho, and D. Son, J. Appl. Phys. **103**, 07A503 (2008).
[16] D. Houssameddine, S. H. Florez, J. A. Katine, J.-P. Michel, U. Ebels, D. Mauri, O. Ozatay, B. Delaet, B. Viala, L. Folks, B. D. Terris, and M.-C. Cyrille, Appl. Phys. Lett. **93**, 022505 (2008).
[17] A. M. Deac, A. Fukushima, H. Kubota, H. Maehara, Y. Suzuki, S. Yuasa, Y. Nagamine, K. Tsunekawa, D. Djayaprawira, and N. Watanabe, Nat. Phys. **4**, 803 (2008).
[18] S. Cornelissen, M. Op de Beeck, L. Lagae, L. Bianchini, and

Joo-Von Kim, T. Devolder, P. Crozat, and C. Chappert, arXiv:0810.1110 (unpublished).
[19] A. Deac, U. Ebels, Y. Liu, O. Redon, M. Li, P. Wang, and B. Dieny, International Conference on Magnetism (ICM), Kyoto, Japan, 2006 (unpublished), presentation TUP2-D-4.
[20] D. Houssameddine *et al.* (unpublished).
[21] Z. Li and S. Zhang, Phys. Rev. B **68**, 024404 (2003).
[22] M. D. Stiles and J. Miltat, in *Spin Dynamics in Confined Magnetic Structures III*, edited by B. Hillebrands and A. Thiaville (Springer, New York, 2006).
[23] A. N. Slavin and V. S. Tiberkevich, Phys. Rev. B **72**, 094428 (2005).
[24] S. Urazhdin, Phys. Rev. B **78**, 060405(R) (2008).
[25] B. Dieny, M. Li, C. Horng, and K. Ju, J. Appl. Phys. **87**, 3415 (2000).
[26] Z. Zhang, L. Zhou, P. E. Wigen, and K. Ounadjela, Phys. Rev. B **50**, 6094 (1994).
[27] J. Z. Sun, Phys. Rev. B **62**, 570 (2000).
[28] J. Grollier, V. Cros, H. Jaffres, A. Hamzic, J. M. George, G. Faini, J. B. Youssef, H. Le Gall, and A. Fert, Phys. Rev. B **67**, 174402 (2003).
[29] J. L. García-Palacios and F. J. Lázaro, Phys. Rev. B **58**, 14937 (1998).
[30] *Non-Linear Phenomena and Chaos in Magnetic Materials*, edited by P. E. Wigen (World Scientific, Singapore, 1994).
[31] G. Bertotti, C. Serpico, I. D. Mayergoyz, A. Magni, M. d'Aquino, and R. Bonin, Phys. Rev. Lett. **94**, 127206 (2005), and references therein.
[32] Z. Yang, S. Zhang, and Y. C. Li, Phys. Rev. Lett. **99**, 134101 (2007).
[33] J. V. Kim, V. Tiberkevich, and A. N. Slavin, Phys. Rev. Lett. **100**, 017207 (2008).
[34] P. Grünberg, M. G. Cottam, W. Vach, C. Mayr, and R. E. Camley, J. Appl. Phys. **53**, 2078 (1982); L. Giovannini, J. M. V. Ngaboyisonga, and F. Nizzoli, Phys. Rev. B **57**, 7438 (1998).
[35] F. M. de Aguiar, A. Azevedo, and S. M. Rezende, Phys. Rev. B **75**, 132404 (2007).
[36] U. Ebels, D. Houssameddine, I. Firastrau, D. Gusakova, C. Thirion, B. Dieny, and L. D. Buda-Prejbeanu, Phys. Rev. B **78**, 024436 (2008).
[37] M. R. Pufall, W. H. Rippard, M. L. Schneider, and S. E. Russek, Phys. Rev. B **75**, 140404(R) (2007).
[38] G. Consolo, B. Azzerboni, L. Lopez-Diaz, G. Gerhart, E. Bankowski, V. Tiberkevich, and A. N. Slavin, Phys. Rev. B **78**, 014420 (2008).
[39] W. H. Rippard, M. R. Pufall, S. Kaka, T. J. Silva, and S. E. Russek, Phys. Rev. B **70**, 100406(R) (2004).
[40] W. H. Rippard, M. R. Pufall, and S. E. Russek, Phys. Rev. B **74**, 224409 (2006).